Mapping glacier basal sliding applying machine learning

Josefine Umlauft[a], Christopher William Johnson[b], Philippe Roux[c], Daniel Taylor Trugman[d], Albanne Lecointre[c], Andrea Walpersdorf[c], Ugo Nanni[e], Florent Gimbert[f], Bertrand Rouet-Leduc[g], Claudia Hulbert[h], Paul Allan Johnson[b]

[a]*ScaDS.AI - Center for Scalable Data Analytics and Artificial Intelligence, Leipzig University, Humboldtstraße 25, Leipzig, 04105, Germany*
[b]*LANL - Los Alamos National Laboratory, Los Alamos, 87545, New Mexico, United States of America*
[c]*ISTerre - Institut des Sciences de la Terre, Maison des Geosciences, Rue du la Piscine 1383, Grenoble, 38041, France*
[d]*University of Nevada, Reno, Nevada Seismological Laboratory, N. Virginia Street, Reno, 1664, Nevada, United States of America*
[e]*University of Oslo, Department of Geosciences, Sem Sælands vei 1, Oslo, 0371, Norway*
[f]*IGE - Institut de Geophysique de l'Environnement, Saint-Martin-d'Heres, Grenoble, 38400, France*
[g]*Disaster Prevention Research Center, Kyoto University, Gokasho, Uji, Kyoto, 611-0011, Japan*
[h]*Ecole Normale Superieure, Paris, France*

Abstract

During the RESOLVE project ("High-resolution imaging in subsurface geophysics: development of a multi-instrument platform for interdisciplinary research"), continuous surface displacement and seismic array observations were obtained on Glacier d'Argentière in the French Alps for 35 days during May in 2018. This unique data set offers the chance to perform a detailed, local study of targeted processes within the highly dynamic cryospheric environment. In particular, the physical processes controlling glacial basal motion are poorly understood and remain challenging to observe directly. Especially in the Alpine region for temperate based glaciers where the ice rapidly responds to changing climatic conditions and thus, processes are strongly intermittent in time and heterogeneous in space. Spatially dense seismic and GPS measurements are analyzed with machine learning techniques to gain insight into the underlying processes controlling glacial motions of Glacier d'Argentière. Using multiple bandpass-filtered copies of the continuous seismic waveforms, we compute energy-based features, develop a matched field beamforming catalogue and include meteorological observations. Features describing the data are analyzed with a gradient boosting decision tree model to directly estimate the GPS displacements from the seismic records. We posit that features of the seismic noise provide direct access to the dominant parameters that drive displacement on the highly variable and unsteady surface of the glacier. The machine learning model infers daily fluctuations as well as longer term trends and the results show on-ice displacement rates are strongly modulated by activity at the base of the glacier. The techniques presented provide a new approach to study glacial basal sliding and discover its full complexity.

Keywords: glacier basal motion, beamforming, machine learning, environmental seismology, cryoseismology

1. Introduction

The cryosphere is one of the most rapidly changing environments on Earth and changes are accentuated by the ongoing evolution of climatic conditions. In mountainous regions, glacier dynamics can be used as a local marker of climate change, and can cause major damage to human infrastructure, so it is of common social interest to study spatiotemporal processes within the ice with high resolution [1]. The rapidly emerging field of "cryoseismology" addresses processes within the glacial environment, such as crevassing, hydrofracturing, failure and calving of ice fragments or supraglacial, englacial and subglacial water discharge via the analysis of continuous seismic records [2]. Special emphasis has been put on the investigation of glacier sliding, which is still not completely understood, but affects large-scale ice flow, ice sheet stability, and thus ultimately sea level rise [3].

Glaciers flow via two processes, internal deformation (or "creep") and basal sliding [4]. The stress-strain relationship for internal deformation of the glacier itself describes viscous deformation associated with ice creep and can be approximated by "Glen's flow law" [5]. Basal sliding is responsible for fast flow of ice-streams; "sliding" is used as an umbrella term here for actual sliding of the ice sole and deformation of soft subglacial till beds (e.g., [6]). In view of steep, unstable ice tongues, it is of great interest to scientists and stakeholders to understand the physical basis of glacier sliding given that catastrophic break-off events threaten mountain communities worldwide [1, 7].

The first theoretical concept of glacier sliding was introduced by postulating that normal forces on undeformable bed undulations produce local shear resistance [8]. Here, a frictionless glacier bed was considered with sliding driven by enhanced deformation and regelation around stiff bed obstacles. Weertman's theory of "hard" bed sliding [8] was modified to account for subglacial water cavity formation [9, 10, 11] and deformable subglacial till layers [12]. Both mechanisms can explain observations of melt-water enhanced ice flow and basal sliding [4]. Modern sliding theories (e.g., [10, 13]) are still influenced by these concepts. However, recent cryoseismological studies show that glacier sliding is not always smooth, but interrupted by distinct slip events [14]. This points to frictional processes, where sudden shear failure at the glacier bed emits seismic waves, analogous to the behavior of tectonic faults. Such stick-slip motion cannot be explained by traditional Weertman-type or soft-bed theories, which describe sliding as a continuous, slow, and smooth process. Instead, frictional processes add to the complexity of basal sliding and thus ice flow. A pivotal challenge in glaciological research is to formulate new or extend existing sliding laws, including conventional concepts but also considering glacier frictional sliding as an additional flow mechanism (e.g., [15, 16, 17, 18, 13]).

Evidence from polar and non-polar ice masses suggests that microseismic stick-slip motion is a widespread and potentially pervasive form of basal sliding (see [2] and references therein; [19, 20, 21, 22, 23, 24]). Individual microseismic stick-slip events are very small with negative magnitudes and shear displacements on millimeter scales or less [25]. Successive events may coalesce into sustained ice-tremor resulting in ice-stream wide sliding episodes with surface displacements of tens of centimeters per day. The spectral signature of the sliding tremor is characterized by spectral peaks at frequencies corresponding to the inverse of inter-event times between individual stick-slip events [26]. First detected at rapid Antarctic ice streams, sliding tremor may be a widespread phenomenon with observational evidence for these sliding tremors beneath Greenlandic [21] and Alpine glacier ice [27], and the slip displacement may be measurable at the ice surface. Detection of these tremors with conventional on-ice seismometers is challenging because the signals can be masked by the extensive glacial noise from other cryoseismic sources, especially englacial and subglacial water flow [28, 21, 29, 27]. Thus, in Alpine regions, with temperate glacier ice and high meltwater production, frictional sliding in the form of microseismic stick-slip tremors may be completely overlooked and far more predominant than presently understood.

Analogous to tectonic faults, stick slip motion across glacial faults emits seismic energy and is commonly measured by seismometers [2]. The frictional state of a tectonic fault and information about the current position within its seismic cycle are still challenging to access. As the fault's rupture, nucleation and magnitude, and future earthquake occurrence are directly controlled by the fault frictional state, its quantification is of interest for understanding the underlying physics [30]. Numerous theoretical simulations and laboratory experiments contributed to the determination of frictional characteristics (e.g., [31, 32, 33, 34, 35, 36]). Recently, analyses of seismic signals from laboratory faults [37] and faults in earth [38] applying machine learning have yielded remarkable results indicating that the seismic waves contain information about the fault characteristics at all times.

We use this analogy to guide the choice of research methodology to monitor the physical state of the glacier. So far, direct and continuous quantification of fault friction cannot be achieved using conventional geophysical approaches, whereas supervised machine learning models are suitable to directly quantify instantaneous fault friction in laboratory experiments and fault properties in tectonic environments [37, 39, 40, 38, 41, 42].

In laboratory experiments it was demonstrated that frictional properties can be accessed through the statistical characteristics of continuous seismic records (range of the data, root mean square, variance, skewness, kurtosis, quantile ranges) [37] and that even different modes of slip along these laboratory faults were captured, which demonstrates that seismic data are a rich archive that allows one to directly observe the physical state of a fault [40]. These processes are similar to basal motion in the glacial environment where the displacement takes place at the ice-bed-interface.

With the aim to uncover the signals related to sliding that are not directly observable, we applied a decision tree model to a new data set from a dense on-ice network on Glacier d'Argentière (French Alps) comprising continuous measurements of local seismicity, surface velocities, and meteorological observations. Due to the highly variable and noisy glacial environment, extensive preprocessing of the seismic and geodetic measurements is essential for a robust feature space with the goal of directly estimating glacier sliding behavior from the surface of the ice and hence, to monitor its dynamics.

2. Methods

2.1. Resolve data collection

As part of the RESOLVE project "High-resolution imaging in subsurface geophysics: development of a multi-instrument platform for interdisciplinary research"), researchers from ISTerre and IGE Grenoble (France) and ETH Zürich (Switzerland) installed a unique sensor infrastructure at the surface of Glacier d'Argentière (Fig. 1) [43]. A dense seismic monitoring array with 98 geophones, 7 GPS stations, a meteorological station, and a water discharge station were operational during approximately one month in May 2018 (24/04/2018-27/05/2018). Five of the GPS stations were installed directly on the surface of the ice (ARG1-ARG4, ARGG) with four of them integrated with the seismic array (ARG1-ARG4). The remaining two stations (ARG5, ARGR) were placed on solid bedrock next to the glacier near the seismic array.

The GPS derived rate of displacement (velocity) was computed for a centered moving time window of size $\pm$ 3 hrs with a 1 hr time step for east, north, and vertical components, and the combined horizontal components (east + north). This sampling was found to provide the best agreement between errors and signal-to-noise ratio (see Fig. A.6 and Fig. A.7 in the Appendix).

Seismic observations were continuously recorded at a sample rate of 500 Hz in a grid-like dense seismic array (Ø 700 m). The stations were deployed into snow about 30 cm below the surface within the ablation zone of Glacier d'Argentière (see [43] for more specific details). Signal preprocessing includes removing the instrument response, detrending and demeaning the continuous waveforms.

Temperature and precipitation were monitored at a 10 min sampling rate using one station situated on solid bedrock about a kilometer to the north of the array. Water discharge was measured every 15 min by the Emosson power supply company in excavated tunnels below the glacier tongue [44, 43].

2.2. Matched Field Processing

Matched field processing (MFP) is the natural extension of plane wave beamforming and yields for the location of seismic noise sources in range, depth and azimuth by analysing spherical waves in the close environment of the underlying seismic array [45]. The approach was originally developed in ocean acoustics [46, 47], but a broad spectrum of applications can be found in environmental seismology to study near-surface processes on the exploration scale [48, 49, 50, 51] and the rapidly emerging special research field of cryoseismology to better understand dynamics within e.g., Alpine glacial ice [52, 22, 27, 53, 54].

Assuming the spatial coherence of the wave field across the array, a systematic correlation of portions of continuous seismic field records and the model-based Green's function (replica) is performed at various candidate source positions. The approach is performed in the frequency domain and can be considered as an equivalent of shift-and-stack techniques in the time domain. For a certain frequency, replica parameterization allows improved data fitting by velocity inversion [55] or polarity optimization for the location of double-couple sources [27]. The procedure is aimed to estimate phase matches between the data wave field and the replica field with the beampower maximum representing the most probable source location.

2.3. Data Features

Data features are statistics of the continuous seismic records from a five-node subarray with high signal-to-noise-ratio, meteorological and water discharge measurements, and events spatially binned from a beamforming catalogue (see Fig. 2 for station locations and a snapshot of the beamforming catalogue).

Statistical features were computed for the continuous seismic record of five selected stations shown as inverted white triangles in Fig. 2. We made four copies of the records using a bandpass filter between 10-50 Hz: 10-20 Hz, 20-30 Hz, 30-40 Hz, and 40-50 Hz to cover the frequency bands related to the most dominant processes in glacial ice, such as water flow, crevassing, icequakes or stick-slip tremors [2]. A moving time window of 1 hr is applied to compute the variance, kurtosis, mean, root mean square, skewness, range and interquantile ranges (0.025, 0.25, 0.5, 0.75, 0.95) using ± 3 hrs before and after the respective time stamp. This sampling matches the GPS data sampling resolution. Hence, statistical features at every hour reflect the distribution of the seismic data within the same 6-hours-windows as the averaged GPS data. The meteorological data (temperature and precipitation) and water discharge measurements are applied by computing the average of 30 data points (meteorological data) / 24 data points (water discharge measurements) corresponding to 6 hrs of seismic data (1 data point is the average of the data during the previous 10 min / 15 min) to obtain consistent feature time windows.

We extracted information from an extensive beamforming catalog which was developed using an advanced matched field processing localization scheme based on a gradient-decent optimization that meets the challenging, seismically "loud" environment. A complete detailed description on the methodology and the MFP implementation can be found in [54]. We used four sub-catalogues with center frequencies of 5 Hz, 10 Hz, 15 Hz and 20 Hz. Each catalogue was thresholded for x,y,z with respect to the dimension of the array and the depth of the glacier as well as for seismic velocities between 1300-3800 $\frac{m}{s}$, as we expect that range to cover Rayleigh wave, P- and S-wave velocities within glacial ice [2]. We additionally reduced each catalogue to normalized beampower values between 0.2-1.0. Fig. 2 shows a 1 hr snapshot of a 10 Hz-catalogue together with the ice surface and the bedrock topography. To use the high-resolution catalogue results as features in the gradient tree boosting model, we spatially binned the MFP derived sources within 8 predefined source regions of the same ice volume (voxels V1-V8). Voxels 1-4 capture the deeper part of the glacier, close to its base, and voxels 5-8 capture the surface equivalent. For each voxel we sum the number of sources and sum their beampower respectively. For consistency with the other data, we apply a moving time window of 1 hr using ± 3 hrs before and after the respective time stamp to match previous feature and label sampling. Virtual cut surfaces and voxel notations are indicated in Fig. 2.

2.4. Xtreme Gradient Boosting Model for Glacier d'Argentière

Gradient tree boosting [56] is a widely used and scalable supervised machine learning approach. It is a very powerful tool that is based on, but usually outperforms, decision tree ensembles [57, 58]. Decision tree ensembles use multiple shallow trees that can be built in a serial manner, in parallel or even independently from each other and combined in a next step in order to enhance model performance. Gradient tree boosting is an extension of decision tree ensembles. The ensemble learner can be used for classification or regression problems. In order to predict a target variable (label), a model is trained based on simple decision rules learned from the data (feature). Depending on the purity of the individual leaves of the tree, the prediction is weighted through a comparison with the respective label. The deviation is represented by an arbitrary loss function. The model is trained sequentially by adding a gradient term to the current decision tree model iteration, with the aim to minimize the loss function for the weighted ensemble of all previous decision trees. Usually, trees that are added in each iteration are shallow (weak learners), but the full ensemble contains a large number of them in total quantity. Once the model is trained, the feature importance can be evaluated to get more insight into the model drivers allowing one to learn which input observations yield the best estimates on the output label [59].

To estimate the GPS velocity on the surface of Glacier d'Argentière, we develop a gradient boosted tree regression model using the features extracted from the data. Specifically, we use the XGBoost implementation from scikit-learn [58, 60]. Model hyperparameters and the choice of feature preprocessing is done by iteratively optimizing the model using 5 fold cross validation on the training data to minimize the average mean-squared-error for the folds. A Bayesian optimizer is implemented for a search space to select the best hyperparameters [61]. The procedure randomly selected hyperparameters for 100 iterations then gradient descent is applied to converge on the best selection for an additional 100 iterations. Initially the search space is large, then expanded or narrowed for specific parameters to avoid final values converging at the upper and lower limits. For each optimization run the evolution of parameters is viewed to update the search space, then the procedure is repeated. The workflow is distributed on a GPU server to train multiple models with different hyperparameters simultaneously to select the final model based on convergence.

We assess the ability of the model to predict the velocity time series of all available RESOLVE GPS stations individually as well as averages of station pairs. We apply a 50%/50% train/test split to our monitoring time series, then perform model training on the first half of the data (16 days) and subsequently test it on the remaining half (16 days), which has not been analyzed before. Model estimates are presented for the three GPS stations that yield the highest prediction scores: ARG2, ARG3 and ARGG (Fig. 1).

2.5. Model development and optimization

Feature preprocessing involved standard scaling (S), quantile transformation (Q) ($n\_quantiles = 50$), principal component analysis (P) ($n\_components = 50$, $whiten = True$), and a random forest regressor (R) ($n\_estimators = 200$, $max\_depth = 3$, $n\_features\_to\_select = 20$, $step = 1$). All routines are available in the scikit-learn package [60, 62]. We optimized the hyperparameters using the original data and for each possible combination of S, Q, P and R. The results show that the best-fit model hyperparameters with the lowest loss function, hence, the best model, strongly depends on the choice and combination of feature preprocessing. For each GPS velocity time series we select preprocessing and accordingly apply the respective model hyperparameters which yield the highest possible prediction score. Comparison of data preprocessing and best-fit model are expressed through the coefficient of determination (R^2) and the correlation-coefficient (CC). These metrics are applied to allow direct comparison between models and do not reflect the absolute quality of the results since a direct correlation is not expected or obtained. To further improve predictions, we tested different applications of a low-pass filter to the GPS velocity time series to reduce the high-frequency 'spiky' fluctuations inherent to the time series. The cutoff frequency was optimized to maximize the evaluation score.

3. Results

The final predictions with the best-fit model hyperparameters, preprocessing, and low-pass filters applied are shown in Figs. 3-5 for GPS station ARG2, ARG3 and ARGG. The training and testing GPS velocity is shown with the data curve in red and the model predictions in blue. For the testing set, the data versus model predictions are shown in the inset.

Comparing the models in terms of hyperparameters, preprocessing, and low-pass filtering indicates the requirements for the best prediction score ($CC = 0.25 - 0.46$) are fundamentally different and significantly influence the model performance (Appendix, Fig. A.8, A.9). For GPS station ARG2, which was located within the seismic array and situated close to seismic node 64 (Fig. 2), we derive a model score of CC = 0.25 with preprocessing P and a low-pass filter with a cutoff frequency of 2.5 hrs applied (see Table 1 for best-fit model hyperparameters). The feature importance shows that statistical features of node 12 contributed most to the model, but that the variance of the 10-20 Hz bandpass filtered record of node 30 has the strongest influence. Those frequencies are sensitive to subglacial water flow, icequake activity and basal stick-slip [2]. It is important to note that node 12 and node 30 were both situated on the north-western flank of the glacier while ARG2 was located in the central-north close to the glacier tongue. The interstation distance and the model's decision "against" favoring features from the closest node 64 posit that the surface velocity of the ice is likely not locally driven by e.g., an opening crevasse, but rather controlled by some seismic activity along the north-western flank.

GPS station ARG3 was situated in line with ARG2 and integrated with the seismic array as well. More precisely it is located next to seismic node 60. We derive a model score of CC = 0.46 with preprocessing S, Q, P and R and a low-pass filter with a cutoff frequency of 16.5 hrs applied (see Table 1 for best-fit model hyperparameters). When comparing to ARG2, more preprocessing and a stronger filter are applied. As a results of the smoother GPS data from the low-pass filter data and model show an almost doubled correlation coefficient. As revealed by the feature importance and as for ARG2, statistics from node 12, situated at the north-western flank of the glacier, are of upmost importance.

For GPS station ARGG situated within the accumulation zone of the glacier <3 km north-west from the seismic array, the best model score is CC = 0.37 with a low-pass filter with a cutoff frequency of 1.39 hrs applied (see Table 1 for best-fit model hyperparameters). The data features were best suited in the original format (no preprocessing) using only a gentle filter to suppress short-term dynamics. The feature importance indicates that beamforming features are most influential for the model, especially source locations from bottom voxel V4 in the 20 Hz filter band which is mostly sensitive to crevassing, icequakes and basal stick-slip [2]. Statistics contributed from stations across the entire array with node 30 leading the rank right after beamforming voxel V4. V4 directly locates beneath node 30, again positing the GPS velocity is being driven by some process at the north-western flank of the glacier, but specifying it to the lower part of the ice close to the glacier's base.

The model outcomes and their related feature ranks for the three GPS stations analyzed show consistent results that suggest glacial surface velocity is being controlled by activity at the north-western flank of the glacier. While for ARG2 and ARG3, situated in the noise-prone ablation zone of the glacier, statistical features from seismic nodes 12 and 30 lead the ranking, the model clearly identifies in-depth activity based on the beamforming features within lower voxel V4 for estimates of ARGG within the accumulation zone. Interestingly, the meteorological features and surface beamforming voxels generally play a subordinate role for the model estimates.

4. Discussion

The application of machine learning using continuous seismic records continues to show success in describing physical processes of complex natural systems. While the glacier motion model predictions are not as robust as those for laboratory stick-slip studies [37, 63, 64, 65, 42], slow slip in Earth [66], future prediction [67, 68], or stick-slip processes in Earth [38], they are nonetheless predictive, especially when describing the long period behavior. Ice deformation is considered mostly aseismic through viscous creep [43], which is inherent to the material properties. The data features are designed to capture such deformation using information in the continuous signal emitted from internally deforming slip boundaries during viscous flow, which occurs at a range of pressures and temperatures. The glacial system dynamics are highly complex and variations in signals produced by the sources of noise appear to be more heterogeneous than in a laboratory system or an earthquake fault.

This study shows for the first time that surface displacement rates can be linked to distinct areas, and even in-depth activity, of a temperate Alpine glacier based on the seismic beamforming features. The addition of seismic beamforming as a data feature provides additional information to the model space and enables the estimate of surface displacement rates on Alpine glacial ice in an highly dynamic and noise-prone environment, and the ability to locate its driving process. To our current state of knowledge, basal motion is most likely the driver for deep cryoseismogenic processes which drive the displacement rates at the surface of Glacier d'Argentière and outrivals internal deformation through viscous creep due to its strong seismic fingerprint [2].

The best model captures the long wavelength characteristics, suggesting that the highly variable temporal fluctuations are generated by a number of incoherent processes and the model can not isolate into these unique characteristics in the feature space. A possible cause is the seismic features contain a combination of information from multiple weak processes and expanding the feature space might improve the high frequency estimates. With the current best model and features, the surface ice velocity can be predicted with an accuracy of up to 46 % for the longer term behavior in the range of 16.5 hrs. Intensively studying the hyperparameter space and the dependence on different choices of preprocessing and low-pass filters shows that each station-related model has to be tuned independently and model settings may not be generalized in the Alpine cryospheric environment. We found that individual station estimates generally score better than averages of multiple on-ice velocity time series and that bedrock stations were less suited for the analysis.

The RESOLVE experiment design was most advantageous for capturing the spatio-temporal seismic and geodetic behavior driven by glacial processes in the one month of data collection. Limitations to the seismic and geodetic measurements as applied to this analysis include the discrepancy in sampling rate (500 Hz for seismic observations vs. 1 hr for geodetic observations). This mismatch requires several steps of preprocessing to properly align the data features and labels, specifically the moving time window analysis and smoothing of the time series data or the compilation of the highly resolved beamforming catalogue. Those procedures come with a potential loss of information regarding short-term variations of the glacier's activity. Furthermore, seismic observations were solely collected in the ablation zone of the glacier, while GPS station coverage spanned over the entire length of Glacier d'Argentière (<3 km). The accumulation zone of temperate based glacial ice is typically less active than the ablation zone. The ablation zone, however, is characterized by a multitude of physical processes such as crevasse formation, meltwater flow or avalanches and rockfalls provoked by increasing temperatures in lower altitudes [54]. Even though the geodetic observations show coherent behavior across the network and the glacier's extent (Fig. A.13), model predictions of distant stations which were situated in the accumulation zone may be challenged due to regime differences. Compared to predictions made on GPS stations which were integrated with the seismic array, model estimates of high-altitude geodetic observations show reasonable performance, but might have benefited from nearby seismic observations.

The mild power threshold of the beamforming catalogue (0.2-1.0) subsequently leads to the integration of poorly resolved seismic sources in our analysis which poses the risk to decrease the model performance due to random, physically unconstrained locations. However, in view of the high noise level in Alpine glacial environments, locations with a lower resolution likely carry relevant information from deep processes at the glacier bed, as e.g. basal stick-slip [27] or subglacial water flow [69]. As revealed by the feature importance for model estimates of GPS ARGG (Fig. 5) the 20 Hz beamforming catalogue as applied to this analysis carries information enabling the best model prediction. The surface displacement itself but also the center frequency of the catalogue reasons that glacier basal motion, potentially coupled with subglacial water flow, is most likely the driving mechanism for the displacement of ARGG, as pure subglacial water flow is characterized by lower frequencies (3-7 Hz) [69] and does not ultimately lead to surface displacement.

We have learned that this line of analysis could potentially contribute to an improvement of glacial sliding laws by considering relevant drivers for model parameterizations that are revealed by the feature importance.

5. Conclusions

A profound understanding and the formulation of sliding laws for glacier basal motion are still a major challenge for the scientific community and needed for hazard assessment and the generation of new prediction models. Especially for temperate glaciers in Alpine regions, sliding is difficult to monitor with conventional geophysical approaches. On-ice seismological records prove to be a very rich archive of glacial activity, but due to glacial noise from other cryoseismic sources, stick-slip events and tremors are often masked and remain unnoticed. New approaches are needed which involve on-ice seismological measurements densely sampled in space and time, as well as modern tools that efficiently analyze such large datasets and reveal previously hidden signals.

We applied the supervised ML approach gradient tree boosting to a seismic array data set acquired in course of the RESOLVE project on Glacier d'Argentière and showed its general suitability for the identification of seismic signatures of ice beds in the presence of melt-induced microseismic noise. The analysis is designed to verify if model estimates are driven by basal motion. Our results demonstrate that gradient tree boosting is a suitable tool to estimate ice surface displacement rates from seismic data collected at glaciers and that information about basal processes can be accessed from on-ice seismometers, analogous to frictional behavior of tectonic fault zones, at least at long period. We have learned that other than for quiet laboratory faults [37] or reasonably long monitoring time series along tectonic faults [39, 38], using only statistical properties of continuous seismic records are not sufficient to describe glacial environments. We adapted the ML model by creating expressive beamforming features using array processing that meet the challenging, seismically "loud" environment. As revealed by the feature importance, the spatio-temporal compilation of seismic source locations provides the essential information for the model to relate estimates of surface velocities to in-depth activity.

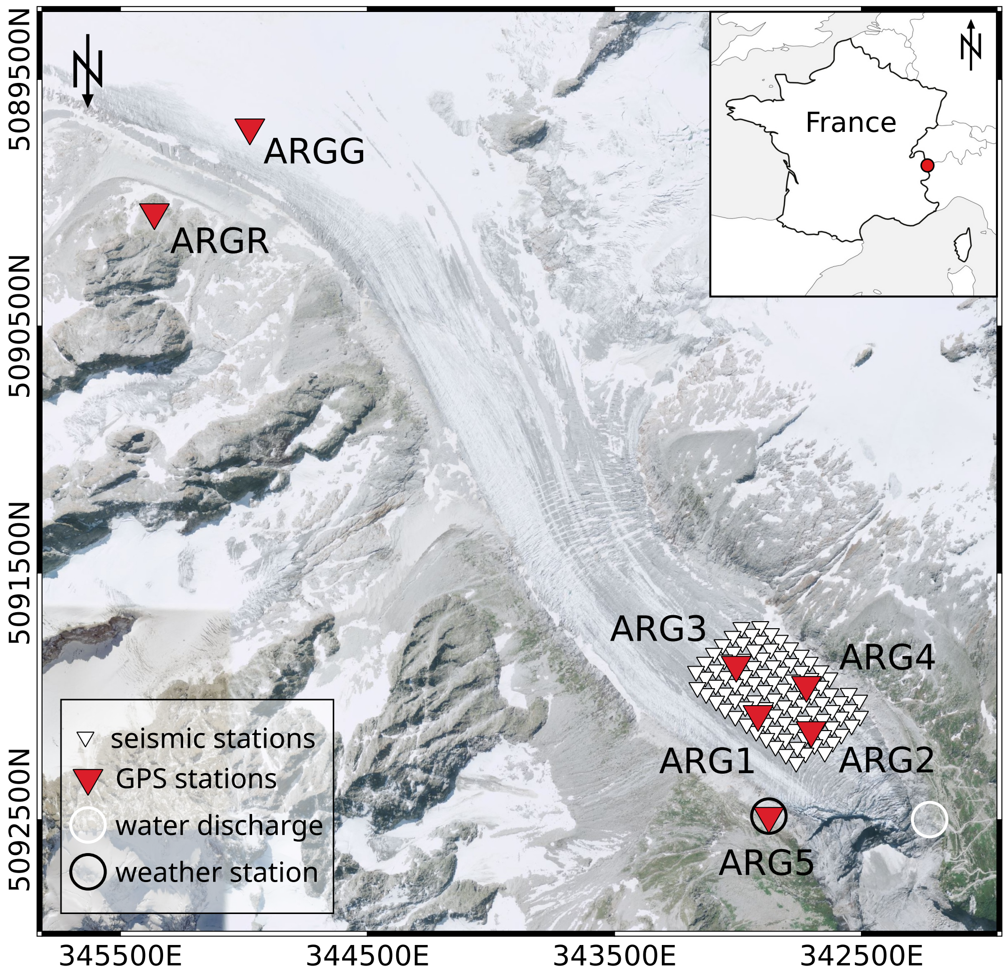

Figure 1: Overview map of Glacier d'Argentière together with the RESOLVE sensor infrastructure [43] including the locations of the seismic nodes (white triangles), the GPS stations (red triangles, ARGx), the weather station (black circle around ARG5) and the location of the borehole for measurements of water discharge (white circle). The GPS stations ARG1, ARG2, ARG3, ARG5 and ARGG were installed on the surface of the glacier (on-ice stations), GPS stations AGR5 and ARGR were installed on solid ground / bedrock (off-ice stations).

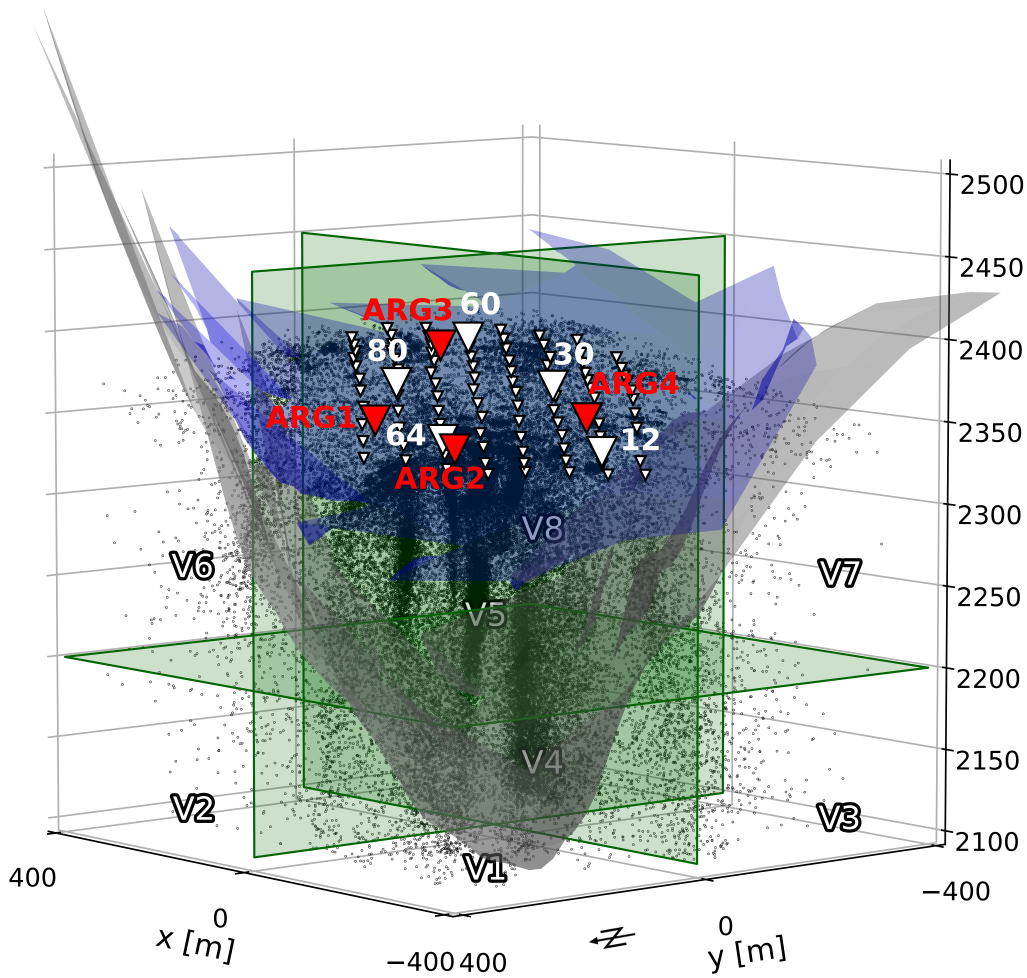

Figure 2: Snapshot of the thresholded beamforming catalogue together with the drone derived ice surface (shades of blue) and the bedrock topography measured by radio-echo sounding (shades of grey). Black dots represent seismic source locations during 1 hr (temporal resolution of 1 sec), for a center frequency of 10 Hz and beampower values between 0.2-1.0. The white triangles indicate the seismic array with the five heightened ones being the selected stations for the computation of the statistical features (12, 30, 60, 64, 80). The red triangles display GPS stations (ARG1-ARG4) situated within the seismic array. The green planes indicate the cut surfaces that divide the glacier into eight voxels (V1-V8) with V1-V4 capturing the lower part close to the glacier bed and V5-V8 encompassing portions of the ice surface.

		GPS stations		
		ARG2	ARG3	ARGG
Hyperparameters	max_depth	5	4	3
	learning_rate	0.052	0.051	0.052
	n_estimators	514	752	527
	gamma	0.816	0.298	0.696
	min_child_weight	1.28	24.803	23.946
	subsample	0.708	0.751	0.738
	colsample	0.771	0.879	0.732
	reg_alpha	9.849	8.349	1.929
	reg_lambda	100.271	147.171	134.623
Preprocessing		P	S,Q,P,R	-
Low-pass filter [hrs]		2.5	16.5	1.39
Correlation-Coefficient		0.25	0.46	0.37

Table 1: Overview of best-fit model hyperparameters, choices of preprocessing and low-pass filters applied to GPS stations ARG2, ARG3, ARGG. The final row holds the prediction scores (see Fig. 3-5 for model performances).

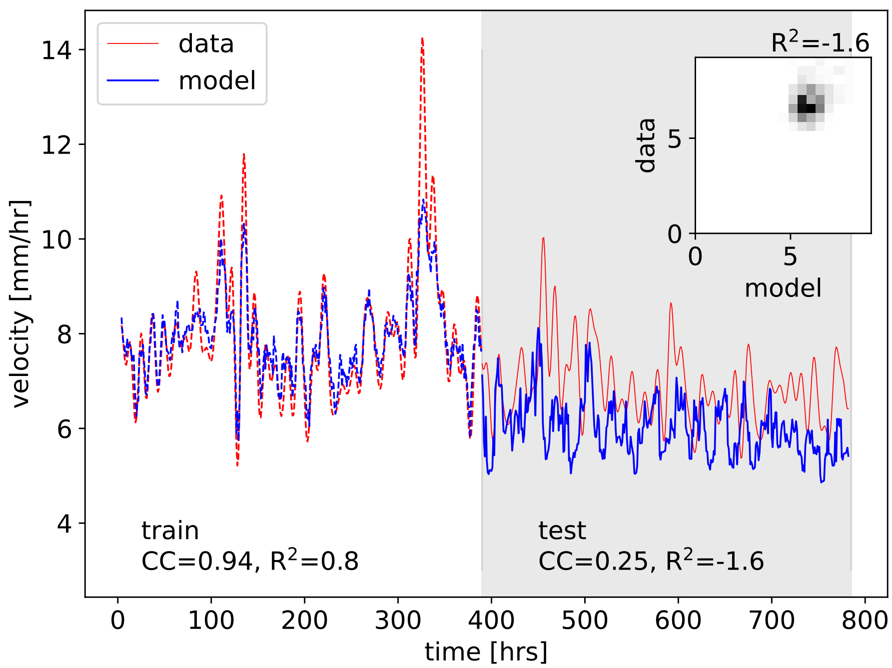

Figure 3: Performance of the XGB model to predict surface velocity [mm/hrs] trained on GPS station ARG2 (see Fig. 1 and Fig. 2), which was situated within the seismic array in the ablation zone of Glacier d'Argentière. The model was trained on 50 % of the monitoring time series (white facecolor) and tested on the remaining 50 %. The GPS velocity (label) is shown in red and the model predictions in blue. The best-fit model hyperparameters are max_depth = 5, learning rate = 0.052, n_estimators = 514, gamma = 0.816, min_child_weight = 1.28, subsample = 0.708, colsample_bytree = 0.771, reg_alpha = 9.849, and reg_lambda = 100.271 with preprocessing = P and a low-pass filter with a cutoff frequency = 2.5 hrs applied.

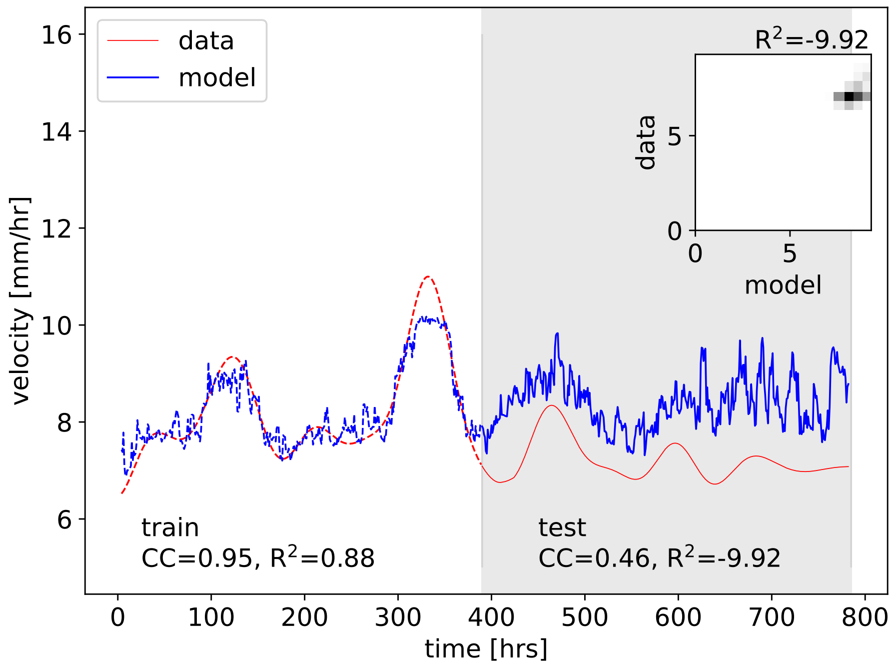

Figure 4: Performance of the XGB model to predict surface velocity [mm/hrs] trained on GPS station ARG3 (see Fig. 1 and Fig. 2), which was situated within the seismic array in the ablation zone of Glacier d'Argentière. The model was trained on 50 % of the monitoring time series (white facecolor) and tested on the remaining 50 %. The GPS velocity (label) is shown in red and the model predictions in blue. The best-fit model hyperparameters are max_depth = 4, learning rate = 0.051, n_estimators = 752, gamma = 0.298, min_child_weight = 24.803, subsample = 0.751, colsample_bytree = 0.879, reg_alpha = 8.349, and reg_lambda = 147.171 with preprocessing = S,Q,P,R and a low-pass filter with a cutoff frequency = 16.5 hrs applied.

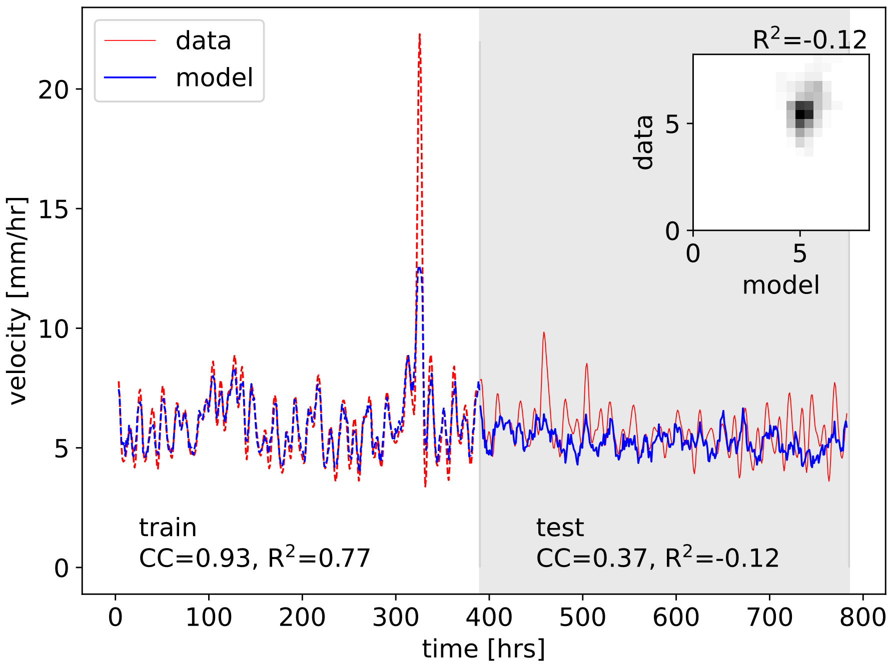

Figure 5: Performance of the XGB model to predict surface velocity [mm/hrs] trained on GPS station ARGG (see Fig. 1 and Fig. 2), which was situated in the accumulation zone of Glacier d'Argentière, about 3 km to the south of the seismic array. The model was trained on 50 % of the monitoring time series (white facecolor) and tested on the remaining 50 %. The GPS velocity (label) is shown in red and the model predictions in blue. The best-fit model hyperparameters are max_depth = 3, learning rate = 0.052, n_estimators = 527, gamma = 0.696, min_child_weight = 23.946, subsample = 0.738, colsample_bytree = 0.732, reg_alpha = 1.929, and reg_lambda = 134.623 with preprocessing = None and a low-pass filter with a cutoff frequency = 1.39 hrs applied.

Appendix A.

The RESOLVE GPS (GNSS) analysis has been performed by a static, differential positioning using the GAMIT software [70] in a network combining the 5 RESOLVE GNSS stations (ARG1-4 on the glacier and ARG5 beside the glacier on the bedrock), plus the ISTerre long-term station ARGG on Glacier d'Argentière outside the RESOLVE network, with 14 permanent and stable RENAG (http://renag.resif.fr) stations in less than 180 km distance (including ARGR on bedrock close to Glacier d'Argentière at 3 km distance from the RESOLVE network). This set of stations has been analyzed in 6-hours-sessions (corresponding to 30-40 mm of displacement of stations on Glacier d'Argentière) shifted by 1 hour to obtain hourly positions for each of the stations. The formal uncertainties of each of the position estimates are 2-3 mm on the horizontal components. The positioning of the bedrock site ARG5, close to the glacier stations and therefore in a comparable environment, indicates a dispersion of 4-6 mm. This value is probably a realistic estimate of the hourly positioning precision of the glacier stations.

Fig. A.6 and Fig. A.7 show the position time series of the the stations ARG2, ARG3 and ARG5.

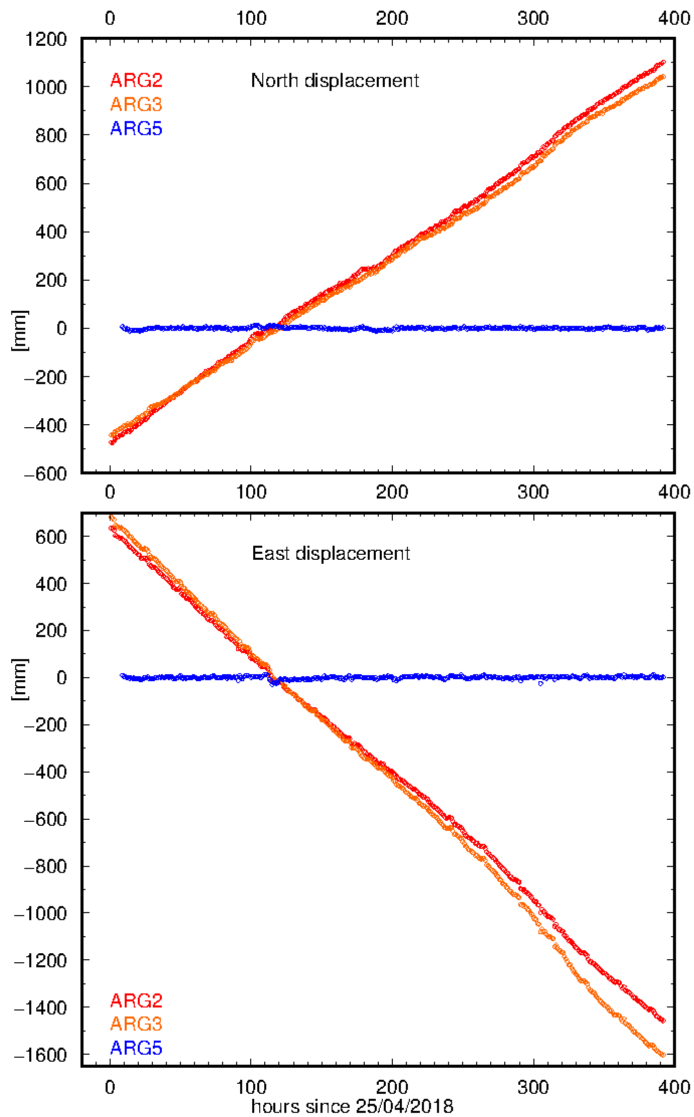

Figure A.6: Rapid evolution of the North and East positions of ARG2 and ARG3 compared to the stable position of ARG5.

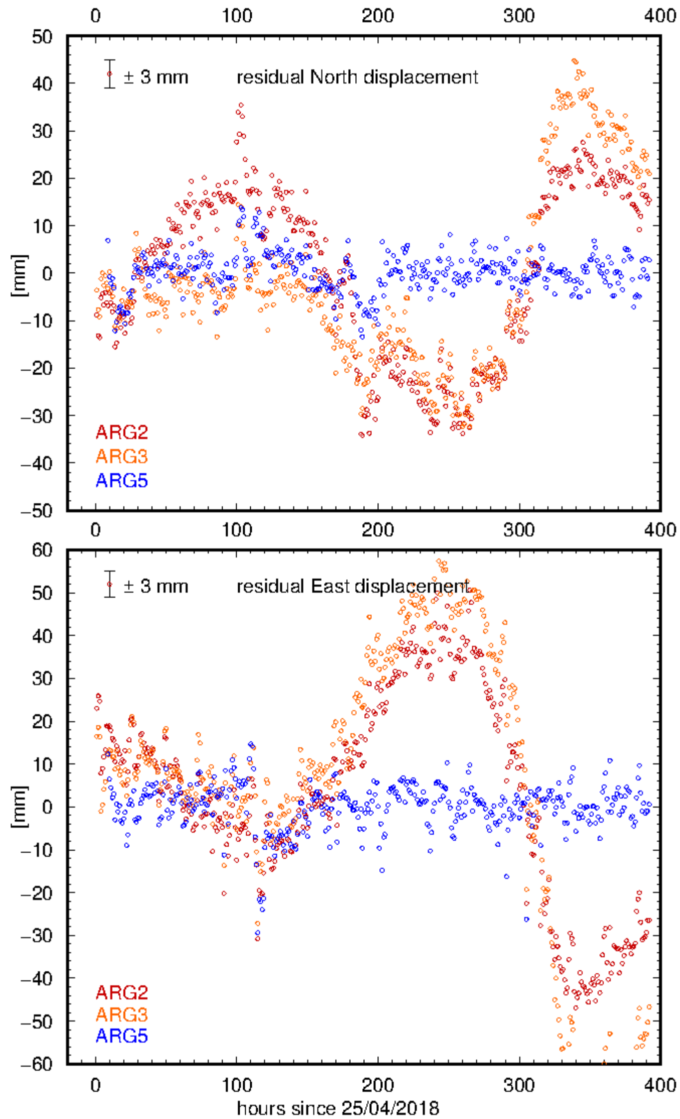

Figure A.7: Displacements of ARG2, ARG3 and ARG5 after linear detrending each component. This highlights the correlated dynamic evolution of ARG2 and ARG3 as well as the dispersion of the hourly positioning results of the stable station ARG5 around their mean value.

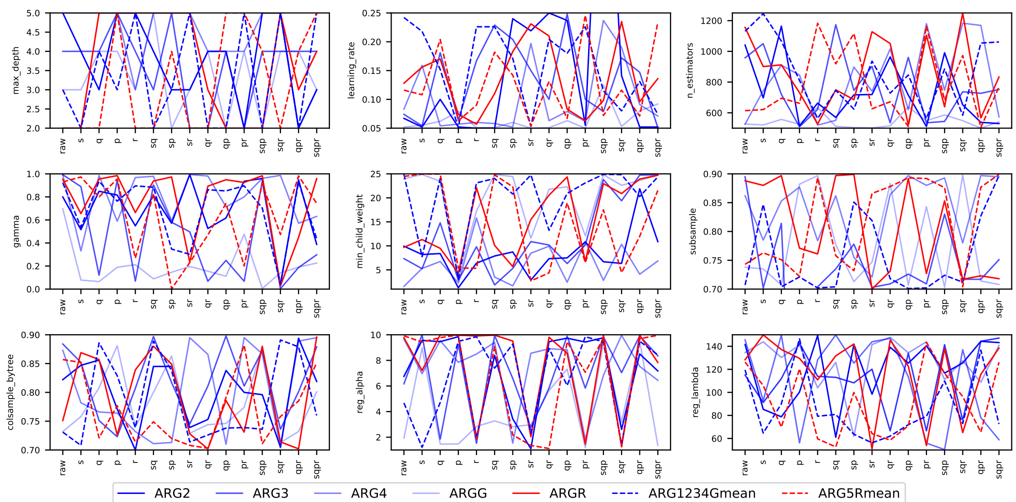

Figure A.8: Hyperparameter optimization for all available GPS stations depending on the choice of preprocessing (S, Q, P, R).

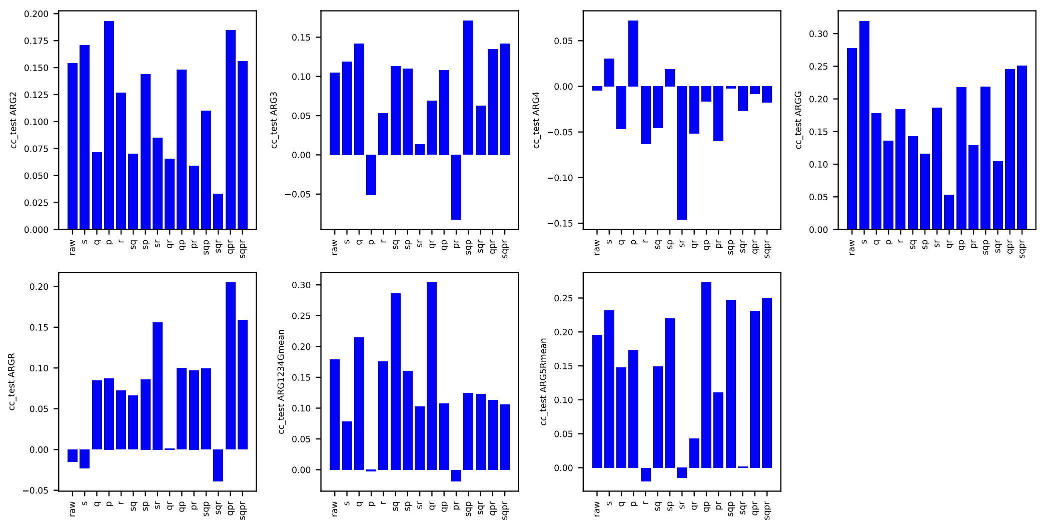

Figure A.9: Model performance for all available RESOLVE GPS stations depending on the choice of preprocessing (S, Q, P, R).

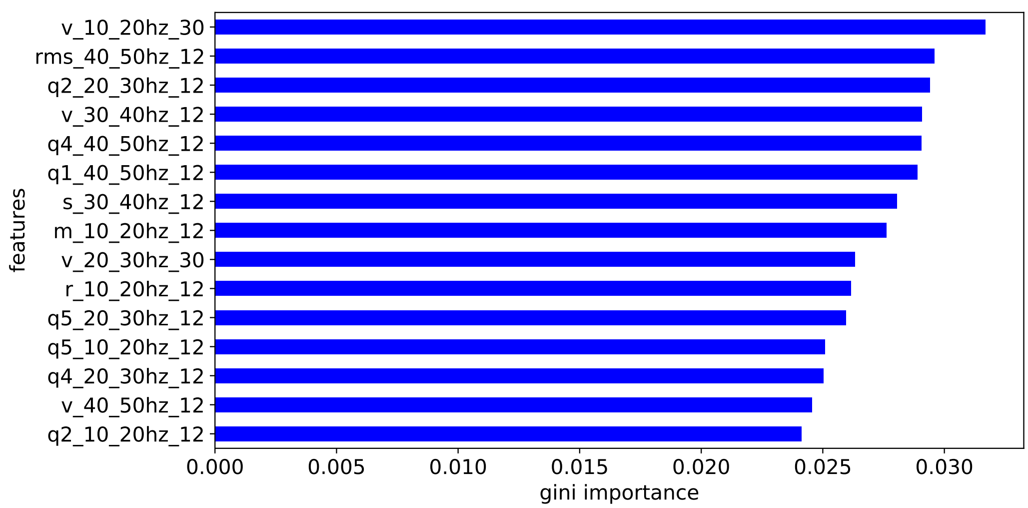

Figure A.10: Gini importance showing the feature importance for model estimates of GPS ARG2 in a decreasing order. The 15 features that contributed most to the model are shown with the most influential ones having a greater value.

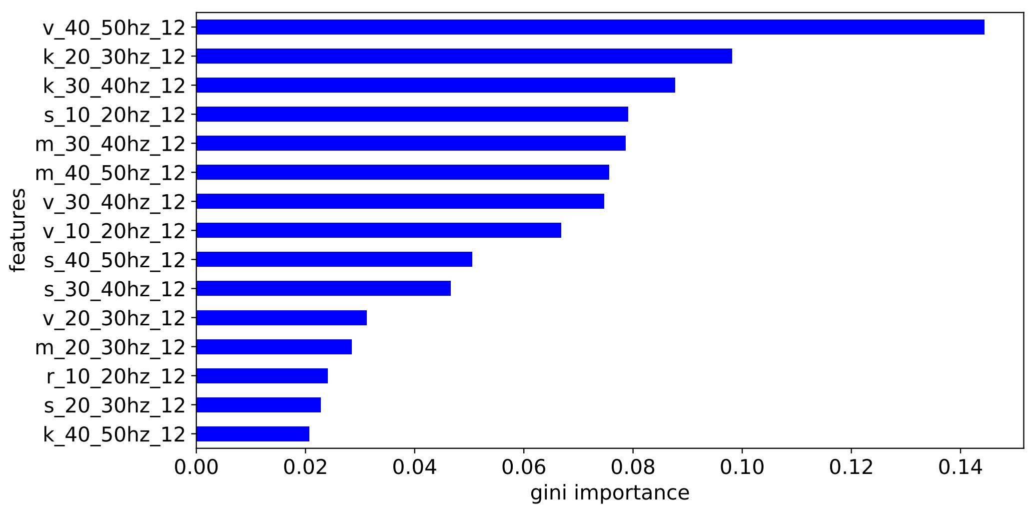

Figure A.11: Gini importance showing the feature importance for model estimates of GPS ARG3 in a decreasing order. The 15 features that contributed most to the model are shown with the most influential ones having a greater value.

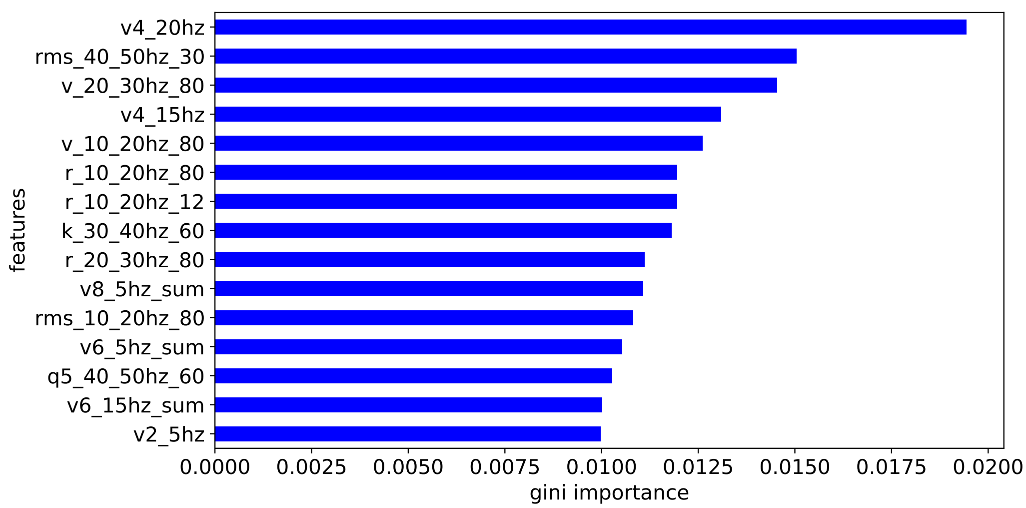

Figure A.12: Gini importance showing the feature importance for model estimates of GPS ARGG in a decreasing order. The 15 features that contributed most to the model are shown with the most influential ones having a greater value.

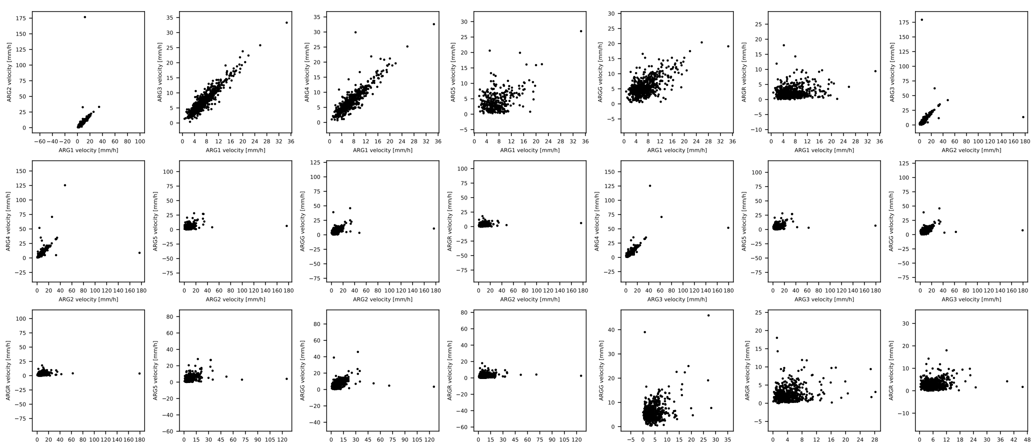

Figure A.13: Station-wise correlation of geodetic observations.

Acknowledgements

The authors acknowledge the financial support by the Federal Ministry of Education and Research of Germany and by the Sächsische Staatsministerium für Wissenschaft Kultur und Tourismus in the program Center of Excellence for AI-research "Center for Scalable Data Analytics and Artificial Intelligence Dresden/Leipzig", project identification number: ScaDS.AI CWJ and PAJ acknowledge support by the U.S. Department of Energy, Office of Science, Office of Basic Energy Sciences, Chemical Sciences, Geosciences, and Biosciences Division under grant 89233218CNA000001. CWJ also acknowledges Institutional Support (Laboratory Directed Research and Development) at Los Alamos National Laboratory. This work has been conducted in the framework of the RESOLVE Project (https://resolve.osug.fr/; LabEx OSUG@2020, Investissement d'avenir – ANR10LABX56 and IDEX Université Grenoble Alpes). The seismic nodes and GPS stations were provided and operated by the French seismological and geodetic network Rèsif-Epos. The computations of the beamforming catalogue were performed using the GRICAD infrastructure (https://gricad.univ-gre-noble-alpes.fr), which is supported by Grenoble research communities, and with the CiGri tool (https://github.com/oar-team/cigri) that was developed by Gricad, Grid5000 (https://www.grid5000.fr) and LIG (https://www.liglab.fr/). The machine Learning model was developed using the resources of the Leipzig University Computing Centre.

Data Availability Statement

The MFP source codes are described and available via https://lecoinal.gricad-pages.univ-grenoble-alpes.fr/resolve/ (last access: 11/11/2021) under a creative commons attribution 4.0 inter- national license. The data derived from the MFP analysis (i.e., 29 sources localizations per second over 34 days and for 20 frequency bands) together with 1 day of raw seismic signal recorded over the 98 seismic stations are available via https://doi.org/10.5281/zenodo.5645545 under a creative commons attribution 4.0 international license (Nanni, Roux, et al., 2021). The complete set of raw seismic data can be found at https://doi.org/10.15778/resif.zo2018 under a creative commons attribution 4.0 international license. The GPS data are available on request through Andrea Walpersdorf (andrea.walpersdorf@univ-grenoble-alpes.fr).

References

[1] J. Faillettaz, M. Funk, C. Vincent, Avalanching glacier instabilities: Review on processes and early warning perspectives , Rev. Geophys. 53 (2015) 203—-224.

[2] E. Podolskiy, F. Walter, Cryoseismology , Reviews of Geophysics 54 (2016) 708–758.

[3] C. Ritz, T. Edwards, G. Durand, A. Payne, V. Peyaud, R. Hindmarsh, Potential sea level rise from Antarctic ice sheet instability constrained by observations , Nature 528 (2015) 115–118.

[4] K. Cuffey, W. Paterson, The Physics of Glaciers , Academic Press (2010).

[5] J. Glen, The creep of polycrystalline ice , Proceeding of the Royal Society of London, Series A 288 (1955) 519–538.

[6] C. Helanow, N. Iverson, J. Woodard, L. Zoet, A slip law for hard-bedded glaciers derived from observed bed topography , Science Advances 7 (20) (2021) 1—-8.

[7] D. Shugar, M. Jaquemart, D. Shean, S. Bhushan, K. Upadhyay, A. Sattar, W. Schwanghart, S. McBride, M. Van Wyk De Vries, M. Mergili, A. Emmer, C. Deschamps-Berger, M. McDonnell, R. Bhambri, S. Allen, E. Berthier, J. Carrivick, J. Clague, M. Dokukin, S. Dunning, H. Frey, S. Gascoin, U. Haritashya, C. Huggel, A. Kääb, J. Kargel, J. Kavanaugh, P. Lacroix, D. Petley, S. Rupper, M. Azam, J. Cook, A. Dimri, M. Eriksson, D. Farinotti, J. Fiddes, K. Gnyawali, S. Harrison, M. Jha, M. Koppes, A. Kumar, S. Leinss, U. Majeed, S. Mal, A. Muhuri, J. Noetzli, F. Paul, I. Rashid, K. Sain, J. Steiner, F. Ugalde, C. Watson, M. Westoby, A massive rock and ice avalanche caused the 2021 disaster at Chamoli, Indian Himalaya , Sciences 373 (6552) (2021) 300—-306.

[8] J. Weertman, On the sliding of Glaciers , Journal of Glaciology 21 (3) (1957) 33–38.

[9] A. Iken, The effect of the subglacial water pressure on the sliding velocity of a glacier in an idealized numerical model , Journal of Glaciology 27 (97) (1981) 407—-421.

[10] C. Schoof, The effect of cavitation on glacier sliding , Proceedings of the Royal Society 461 (2005) 609—-627.

[11] O. Gagliardini, D. Cohen, P. Råbback, T. Zwinger, Finite-element modeling of subglacial cavities and related friction law , Journal of Geophysical Research 112 (2007) 1—-11.

[12] T. Murray, Assessing the paradigm shift: Deformable glacier beds , Quaternary Science Reviews 16 (9) (1997) 995—-1016.

[13] L. Zoet, N. Iverson, A slip law for glaciers on deformable beds , Science 368 (6486) (2020) 76—-78.

[14] R. Aster, R. Winberry, Glacial Seismology , Reports on Progress in Physics 80 (2017).

[15] O. Sergienko, D. MacAyeal, R. Bindschadler, Stick–slip behavior of ice streams: Modeling investigations , Annals of Glaciology 50 (52) (2009) 87—-94.

[16] J. Winberry, S. Anandakrishnan, D. Wiens, Dynamics of stick-slip motion, Whillans Ice Stream, Antarctica , Earth and Planet, Sci. Lett. 305 (2011) 283—-289.

[17] B. Lipovsky, E. Dunham, Slow-slip events on the Whillans Ice Plain, Antarctica, described using rate-and-state friction as an ice stream sliding law , J. Geophys. Res. Earth Surf. 122 (2017) 973—-1003.

[18] B. Lipovsky, C. Meyer, L. Zoet, C. McCarthy, D. Hansen, A. Rempel, F. Gimbert, Glacier sliding, seismicity and sediment entrainment , Annals of Glaciology 60 (79) (2019) 182—-192.

[19] C. Barcheck, S. Tulaczyk, S. Schwartz, J. Walter, J. Winberry, Implications of basal micro-earthquakes and tremor for ice stream mechanics: Stick-slip basal sliding and till erosion , Earth and Planet, Sci. Lett. 486 (2019) 54—-60.

[20] T. Hudson, A. Brisbourne, F. Walter, D. Gräff, R. White, A. Smith, Icequake source mechanisms for studying glacial sliding , Journal of Geophysical Research: Solid Earth 125 (11) (2020).

[21] I. McBrearty, L. Zoet, S. Anandakrishnan, Basal seismicity of the Northeast Greenland Ice Stream , Journal of Glaciology (2020) 1–17.

[22] F. Walter, D. Gräff, F. Lindner, P. Paitz, M. Knöpfli, M. Chmiel, A. Fichtner, Distributed acoustic sensing of microseismic sources and wave propagation in glaciated terrain , Nature Communications 11 (2436) (2020) 1–10.

[23] D. Gräff, M. Knöpfli, B. Lipovsky, P. Selvadurai, D. Farinotti, F. Walter, Fine structure of microseismic glacial stick-slip , Geophysical Research Letters 48 (2021).

[24] S. Kufner, A. Brisbourne, A. Smith, T. Hudson, T. Murray, R. Schlegel, J. Kendal, S. Anandakrishnan, I. Lee, Not all icequakes are created equal: Basal icequakes suggest diverse bed deformation mechanisms at Rutford Ice Stream, West Antarctica , Journal of Geophysical Research: Earth Surface 126 (3) (2021) 1–17.

[25] A. Helmstetter, B. Nicolas, P. Comon, M. Gay, Basal icequakes recorded beneath an Alpine glacier (Glacier d'Argentière, Mont Blanc, France): Evidence for stick-slip motion? , Science 368 (6486) (2020) 76—-78.

[26] B. Lipovsky, E. Dunham, Tremor during ice-strem stick slip , The Cryosphere 10 (2016) 385–399.

[27] J. Umlauft, F. Lindner, P. Roux, D. Mikesell, M. Haney, M. Korn, F. Walter, Stick-Slip Tremor Beneath an Alpine Glacier , Geophysical Research Letters 48 (2021) 1–10.

[28] C. Röösli, F. Walter, S. Husen, L. Andrews, M. Lüthi, G. Catania, E. Kissling, Sustained seismic tremors and icequakes detected in the ablation zone of the Greenland Ice Sheet , Journal of Glaciology 60 (221) (2014) 563–575.

[29] E. Eibl, C. Bean, B. Einarsson, F. Pàlsson, K. Vogfjörd, Seismic ground vibrations give advanced early-warning of subglacial floods , Nature Communications 11 (1) (2020) 1–11.

[30] C. Marone, Laboratory-derived friction laws and their application to seismic faulting , Annual Review of Earth and Planetary Sciences 26 (1) (1998) 643–696.

[31] E. Rabinowicz, Autocorrelation analysis of the sliding process , Journal of Applied Physics 27 (1956) 131–135.

[32] C. Scholz, Microfracturing and the inelastic deformation of rock in compression , Journal of Geophysical Research 73 (4) (1968) 1417–1432.

[33] S. Rubinstein, G. Cohen, J. Fineberg, Detachment fronts and the onset of dynamic friction , Nature 430 (2) (2004) 1005–1009.

[34] B. Kaproth, C. Marone, Slow earthquakes, preseismic velocity changes, and the origin of slow frictional stick-slip , Science 341 (6151) (2013) 1229–1232.

[35] R. Madariaga, S. Ruiz, Earthquake dynamics on circular faults: A review 1970–2015 , Journal of Seismology 20 (4) (2016) 1235–1252.

[36] O. Dorostkar, R. Guyer, P. Johnson, C. Marone, J. Carmeliet, On the micromechanics of slip events in sheared, fluid-saturated fault gouge , Geophysical Research Letters 44 (2017) 6101–6108.

[37] B. Rouet-LeDuc, C. Hulbert, D. Bolton, C. Ren, J. Riviere, C. Marone, R. Guyer, P. Johnson, Estimatig fault friction from from seismic signals in the laboratory , Geophysical Research Letters 45 (2018) 1321–1329.

[38] C. Johnson, P. Johnson, Learning the low frequency earthquake daily intensity on the central san andreas fault, Geophysical Research Letters 48 (15) (2021) e2021GL092951. doi:10.1029/2021GL092951.

[39] B. Rouet-LeDuc, C. Hulbert, P. Johnson, Continuous chatter of the Cascadia subduction zone revealed by machine learning , Nature Geoscience 12 (2018) 75–79.

[40] C. Hulbert, B. Rouet-LeDuc, P. Johnson, C. Ren, J. Riviere, D. Bolton, C. Marone, Similarity of fast and slow earthquakes illuminated by machine learning , Nature Geoscience 12 (2019) 69–74.

[41] C. Ren, A. Peltier, V. Ferrazzini, B. Rouet-Leduc, P. Johnson, F. Brenguier, Machine learning reveals the seismic signature of eruptive behavior at piton de la fournaise volcano, Geophysical research letters 47 (3) (2020) e2019GL085523.

[42] K. Wang, C. Johnson, K. Bennett, P. Johnson, Predicting fault slip via transfer learning, Nature Communications 12 (12 2021). doi:10.1038/s41467-021-27553-5.

[43] F. Gimbert, U. Nanni, P. Roux, A. Helmstetter, S. Garambois, A. Lecointre, A. Walpersdorf, B. Jourdain, M. Langlais, O. Laarman, et al., A multi-physics experiment with a temporary dense seismic array on the argentière glacier, french alps: The resolve project, Seismological Society of America 92 (2A) (2021) 1185–1201.

[44] C. Vincent, L. Moreau, Sliding velocity fluctuations and subglacial hydrology over the last two decades on argentière glacier, mont blanc area, Journal of Glaciology 62 (235) (2016) 805–815. doi:10.1017/jog.2016.35.

[45] H. Bucker, Use of calculated sound fields and matched-field detection to locate sound sources in shallow water, Journal of Acoustical Society of America 59 (2) (1976) 368–373.

[46] A. Baggeroer, Fellow, IEEE, W. Kuperman, P. Mikhalevsky, An Overview of Matched Field Methods in Ocean Acoustics, IEEE Journal of Oceanic Engineering 18 (4) (1993) 401–424.

[47] W. Kuperman, G. Turek, Matched Field Acoustics, Mechanical Systems and Signal Processing 11 (1) (1997) 141–148.

[48] J. Vandemeulebrouck, P. Roux, P. Gouédard, A. Legaz, A. Revil, A. Hurst, A. Bolève, A. Jardani, Application of acoustic noise and self-potential localization techniques to a buried hydrothermal vent (Waimangu Old Geyser site, New Zealand), Geophysical Journal International 180 (2010) 883–890.

[49] E. Cros, P. Roux, J. Vandemeulebrouck, S. Kedar, Locating hydrothermal acoustic sources at Old Faithful Geyser using Matched Field Processing, Geophysical Journal International 187 (2011) 385–393.

[50] M. Corciulo, P. Roux, M. Campillo, D. Dubucq, W. Kuperman, Multiscale matched-field processing for noise-source localization in exploration geophysics, Geophysics 77 (5) (2012) KS33–KS41.

[51] J. Umlauft, M. Korn, 3D fluid channel location from noise tremors using matched field processing , Geophysical Journal International 219 (3) (2019) 1550–1561.

[52] F. Walter, P. Roux, C. Röösli, A. Lecointre, D. Kilb, P. Roux, Using glacier seismicity for phase velocity measurements and Green's function retrieval, Geophysical Journal International 201 (2015) 1722–1737.

[53] U. Nanni, F. Gimbert, P. Roux, A. Lecointre, Observing the subglacial hydrology network and its dynamics with a dense seismic array, Proceedings of the National Academy of Sciences 118 (28) (2021) e2023757118.

[54] U. Nanni, F. Gimbert, P. Roux, A. Lecointre, Dynamic Imaging of Glacier Structures at High-Resolution Using Source Localization With a Dense Seismic Array , Geophysical Research Letters 49 (2022) 1–9.

[55] C. Gradon, L. Moreau, P. Roux, J. Ben-Zion, Analysis of surface and seismic sources in dense array data with match field processing and Markov chain Monte Carlo sampling, Geophysical Journal International 218 (2019) 1044–1056.

[56] J. Friedman, T. Hastie, R. Tibshirani, Additive Logistic Regression: A Statistical View of Boosting , The Annals of Statistics 28 (2) (2000) 337–407.

[57] L. Breiman, Random Forests , Machine Learning 45 (2001) 5–32.

[58] T. Chen, C. Guestrin, XGBoost: A scalable tree boosting system , In Proceedings of the 22nd ACM SIGKDD International Conference on Knowledge Discovery and Data Mining. New York: ACM (2016) 785–794.

[59] A. Müller, S. Guido, Introduction to Machine Learning with Python , Academic Press (2016) 1720–1728.

[60] F. Pedregosa, G. Varoquaux, A. Gramfort, V. Michel, B. Thirion, O. Grisel, M. Blondel, P. Prettenhofer, R. Weiss, V. Dubourg, J. Vanderplas, A. Passos, D. Cournapeau, M. Brucher, M. Perrot, E. Duchesnay, Scikit-learn: Machine learning in Python, Journal of Machine Learning Research 12 (2011) 2825–2830.

[61] T. Head, MeachCoder, G. Louppe, I. Shcherbatyi, fcharras, Z. Vinícius, cmmalone, C. Schröder, nel215, N. Campos, T. Young, T. Cereda, T. Fan, rene rex, K. Shi, J. Schwabedal, carlosdanielcsantos, Hvass-Labs, M. Pak, SoManyUsernamesTaken, F. Callaway, L. Estève, L. Besson, M. Cherti, K. Pfannschmidt, F. Linzberger, C. Cauet, A. Gut, A. Mueller, A. Fabisch, scikit-optimize/scikit-optimize: v0.5.2., Zenodo (2018).

[62] L. Buitinck, G. Louppe, M. Blondel, F. Pedregosa, A. Mueller, O. Grisel, V. Niculae, P. Prettenhofer, A. Gramfort, J. Grobler, R. Layton, J. VanderPlas, A. Joly, B. Holt, G. Varoquaux, API design for machine learning software: experiences from the scikit-learn project, in: ECML PKDD Workshop: Languages for Data Mining and Machine Learning, 2013, pp. 108–122.

[63] P. Shokouhi, V. Girkar, J. Rivière, S. Shreedharan, C. Marone, C. Giles, D. Kifer, Deep learning can predict laboratory quakes from active source seismic data, Geophysical Research Letters 48 (06 2021). doi:10.1029/2021GL093187.

[64] F. Corbi, L. Sandri, J. Bedford, F. Funiciello, S. Brizzi, M. Rosenau, S. Lallemand, Machine learning can predict the timing and size of analog earthquakes, Geophysical Research Letters 46 (2019) 1303 – 1311.

[65] H. Jasperson, D. Bolton, P. Johnson, R. Guyer, C. Marone, M. de Hoop, Attention network forecasts time-to-failure in laboratory shear experiments, Journal of Geophysical Research: Solid Earth 126 (11 2021). doi:10.1029/2021JB022195.

[66] C. Hulbert, B. Rouet-Leduc, R. Jolivet, P. Johnson, An exponential build-up in seismic energy suggests a months-long nucleation of slow slip in cascadia, Nature Communications 11 (2020) 4139. doi:10.1038/s41467-020-17754-9.

[67] L. Laurenti, E. Tinti, F. Galasso, L. Franco, C. Marone, Deep learning for laboratory earthquake prediction and autoregressive forecasting of fault zone stress, Earth and Planetary Science Letters 598 (2022) 117825. doi:https://doi.org/10.1016/j.epsl.2022.117825.
URL `https://www.sciencedirect.com/science/article/pii/S0012821X22004617`

[68] K. Wang, C. Johnson, K. Bennett, P. Johnson, Predicting future laboratory fault friction through deep learning transformer models, Geophysical Research Letters 49 (10 2022). doi:10.1029/2022GL098233.

[69] U. Nanni, F. Gimbert, C. Vincent, D. Gräff, F. Walter, L. Piard, L. Moreau, Quantification of seasonal and diurnal dynamics of subglacial channels using seismic observations on an alpine glacier, The Cryosphere 14 (5) (2020) 1475–1496.

[70] T. Herring, R. King, F. M.A., S. McClusky, Gamit reference manual, gps analysis mit, release 10.7, Department of Earth, Atmospheric and Planetary Sciences, Masssachusetts Institute of Technology, Cambridge, MA (2018).